Core−Shell Gyroid Morphology in a Poly(isoprene-*block*-styrene-*block*-dimethylsiloxane) Triblock Copolymer

T. A. Shefelbine,[†] M. E. Vigild,[†] M. W. Matsen,[‡] D. A. Hajduk,[§] M. A. Hillmyer,[⊥] E. L. Cussler,[†] F. S. Bates*,[†]

Contribution from the Department of Chemical Engineering and Materials Science and Department of Chemistry, University of Minnesota, Minneapolis, Minnesota 55455, Polymer Science Centre, University of Reading, Whiteknights, Reading, U.K. RG6 6AF, and Symyx Technologies, Santa Clara, California 95051

Received May 3, 1999

Abstract: We report a new morphology in a poly(isoprene-*block*-styrene-*block*-dimethylsiloxane) ABC triblock copolymer. The most probable symmetry of the morphology ($Ia\bar{3}d$) was determined from two-dimensional SAXS measurements performed on a sample with long-range order induced by an oscillatory shear field. By comparing the predictions of self-consistent field theory with TEM and SAXS and SANS powder diffraction patterns, we deduced that the morphology is a core−shell gyroid comprised of two independent and triply periodic poly(dimethylsiloxane) networks encased in poly(styrene) shells and separated by a continuous poly(isoprene) domain. Thus, this unique nanostructure divides space into five independent, three-dimensionally continuous domains.

Introduction

Over the past few years, researchers have achieved a detailed understanding of the microphase-separated morphologies of AB diblock copolymer melts.[1,2] The connectivity of the A and B blocks requires the molecules to stretch in order to separate into A- and B-rich domains. Thus, the domains remain microscopic in size, and an extensive amount of A/B internal interface results. To balance the stretching energy between A and B blocks, the interface acquires a spontaneous curvature that increases in magnitude as the molecule becomes asymmetric. The increasing spontaneous curvature causes the well-known progression of classical morphologies from lamellae to cylinders to spheres.[3] At the boundary between cylinders and lamellae, a number of complex morphologies possess a more favorable interfacial curvature. However, only one, the gyroid phase, is stable because it possesses the lowest amount of packing frustration.[4] Packing frustration occurs when the interface is unable to produce uniformly thick domains while at the same time having a uniform interfacial curvature. The uniform domain thickness is necessary for minimizing the stretching energy, and the uniform curvature minimizes the interfacial area.

During these advances in the understanding of diblock copolymer phase behavior, preliminary studies illustrated that the behavior becomes far more elaborate with the addition of a third dissimilar block.[5−7] Although the same simple principles developed for AB diblock molecules also apply to ABC triblock copolymers, anticipating the behavior becomes far more difficult. ABC triblock copolymer morphologies must minimize the stretching energy from three different domains and the interfacial energy from (potentially) three distinct interfaces.[8,9] Furthermore, the sequence of domains must correspond to the sequence of blocks in the molecule. For a linear ABC triblock, this means a B-rich domain must be in contact with both A- and C-rich domains.

The additional complexity of ABC triblock copolymer behavior is reflected in a much richer complement of morphologies. While the AB diblock architecture affords access to only four distinct equilibrium ordered states, it is evident that ABC triblock copolymers can display many distinct morphologies.[5,6,7] If we are able to master their behavior, the ABC triblock could become a far more useful architecture than the simple AB diblock. For example, the available patterns for nanolithographic

* To whom correspondence should be addressed.
[†] Department of Chemical Engineering and Materials Science, University of Minnesota.
[‡] University of Reading.
[§] Symyx Technologies.
[⊥] Department of Chemistry, University of Minnesota.

(1) Khandpur, A. K.; Förster, S.; Bates, F. S.; Hamley, I. W.; Ryan, A. J.; Bras, W.; Almdal, K.; Mortensen K. *Macromolecules* **1995**, *28*, 8796−8806.
(2) Matsen, M. W.; Bates, F. S. *J. Chem. Phys.* **1997**, *106*, 2436−2448.
(3) Leibler, L. *Macromolecules* **1980**, *13*, 1602−1617. Semenov, A. N. *Sov. Phys. JETP* **1985**, *61*, 733−742.
(4) Matsen, M. W.; Bates, F. S. *Macromolecules* **1996**, *29*, 7641−7646.
(5) Mogi, Y.; Kotsuji, H.; Kaneko, Y.; Mori, K.; Matsushita, Y.; Noda, I. *Macromolecules* **1992**, *25*, 5408−5411. Mogi, Y.; Nomura, M.; Kotsuji, H.; Ohnishi, K.; Matsushita, Y.; Noda, I. *Macromolecules* **1994**, *27*, 6755−6760. Matsushita, Y.; Suzuki, J.; Seki, M. *Physica B* **1998**, *248*, 238−242.
(6) Mogi, Y.; Mori, K. Kotsuji, H.; Matsushita, Y.; Noda, I.; Han, C. *Macromolecules* **1993**, *26*, 5169−5173. Gido, S.; Schwark, D.; Thomas, E.; Goncalves, M. *Macromolecules* **1993**, *26*, 2636−2640.
(7) Auschra, C.; Stadler, R. *Macromolecules* **1993**, *26*, 2171−2174. Stadler, R.; Auschra, C.; Beckmann, J.; Krappe, U.; Voigt-Martin, I.; Leibler, L. *Macromolecules* **1995**, *28*, 3080−3097. Krappe, U.; Stadler, R.; Voigt-Martin, I. *Macromolecules* **1995**, *28*, 4558−4561. Breiner, U.; Krappe, U.; Abetz, V.; Stadler, R. *Macromol. Chem. Phys.* **1997**, *198*, 1051−1083. Brinkmann, S.; Stadler, R.; Thomas, E. *Macromolecules* **1998**, *31*, 6556−6572. Breiner, U.; Krappe, U.; Jakob, T.; Abetz, V.; Stadler, R. *Polym. Bull.* **1998**, *40*, 219−226. Breiner, U.; Krappe, U.; Thomas, E.; Stadler, R. *Macromolecules* **1998**, *31*, 135−141.
(8) Matsen, M. W. *J. Chem. Phys.* **1998**, *108*, 785−796.
(9) Nakazawa, H.; Ohta, T. *Macromolecules* **1993**, *26*, 5503−5511. Zheng, W.; Wang, Z. G. *Macromolecules* **1995**, *28*, 7215−7223. Phan, S.; Fredrickson, G. H. *Macromolecules* **1998**, *31*, 59−63.

10.1021/ja991442h CCC: $18.00
Published on Web 09/03/1999

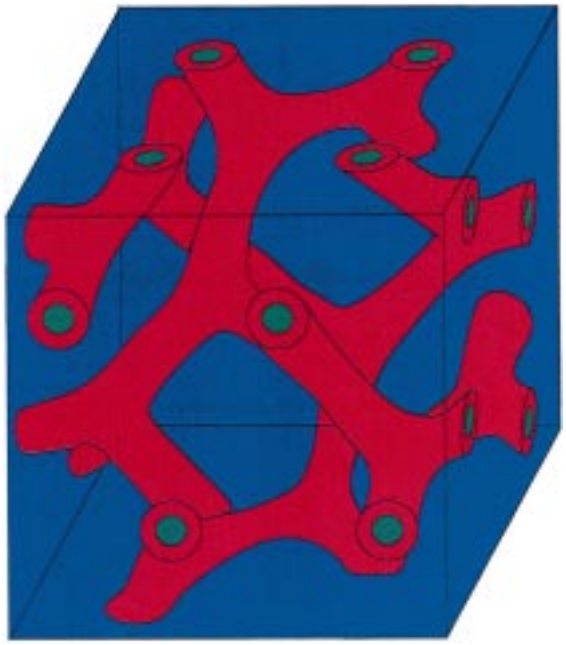

Figure 1. Schematic illustration of the core-in-shell gyroid structure associated with the poly(isoprene-*block*-styrene-*block*-dimethylsiloxane) (ISD) triblock copolymer; blue, red, and green regions correspond to I, S, and D domains, respectively. This schematic is included for the conceptual understanding of the reader in relation to the familiar depiction of the gyroid morphology.[31] It does not accurately portray the volume fractions of the reported structure (see Figure 7).

techniques could be vastly increased.[10] Our immediate motivation for examining ABC triblocks is to produce membranes for gas separation. To do this, we chose a glassy center block and two rubbery end blocks; a poly(isoprene-*block*-styrene-*block*-dimethylsiloxane) (ISD) triblock satisfies these requirements. The membrane should allow a gas mixture to enter one of the rubbery domains (e.g., D), to pass through the glassy S domain, which acts as a selective separation layer, and to exit the membrane through the other rubber domain (e.g., I). For this membrane to work, the S domain must completely separate the I and D domains, and each of the three domains must span the copolymer sample.

In general, ABC triblock morphologies are much more intricate than those produced by AB diblocks and, therefore, require more sophisticated characterization methods. Identification of the morphology reported here required a combination of various experimental and theoretical techniques, including small-angle X-ray and neutron scattering (SAXS and SANS), a shear orienting technique, transmission electron microscopy (TEM), and self-consistent field theory (SCFT) calculations. Implementing this complement of techniques allowed us to identify one of the most complicated block copolymer morphologies reported to date.

The ISD triblock copolymer studied in this report has volume fractions of 0.40/0.41/0.19, respectively and a molecular weight of 41 000 g/mol. We show that the morphology of this triblock is a core−shell gyroid structure with an $Ia\bar{3}d$ space-group symmetry. Figure 1 depicts the unit cell in a schematic that is similar to a typical rendition of the gyroid morphology for AB diblock copolymers. The structure consists of two D cores (shown in green) forming two lattices of three-fold connectors in a gyroid network. Covering each lattice is a shell of S (shown in red), and the surrounding matrix is composed of I (shown in blue), resulting in five distinct domains, each spanning three-dimensional space. Thus, we term this triply periodic cubic structure the pentacontinuous core−shell gyroid phase. In contrast, the AB[11] and ABC[5,8] gyroid phases identified earlier are tricontinuous. This particular morphology satisfies the requirements necessary for our proposed gas separation membrane.

Experimental Section

Synthesis. The ISD triblock copolymer described in this report was synthesized by sequential anionic polymerization of isoprene, styrene, and hexamethylcyclotrisiloxane (D_3) using techniques and equipment described elsewhere.[12] Isoprene (10.4 g) was initiated with *sec*-butyllithium and polymerized at 40 °C in cyclohexane; these conditions are known to produce 95% 4,1 addition.[13] After 4 h, the time estimated for greater than 99% conversion, the living poly(isoprenyllithium) solution was cooled to 6 °C, and 18 mL of rigorously purified THF, followed by 12.9 g of styrene, was added to the reactor. THF facilitates rapid crossover from poly(isoprenyllithium) to poly(stryllithium). Under these polar conditions, the styrene monomer is know to polymerize rapidly.[14] We allowed the styrene to react for approximately 30 min. Subsequently, the living solution was warmed to 22 °C, and 10.2 g of D_3, dissolved in approximately 17 mL of THF, was added to the reaction medium. Within 30 min, the reddish-orange color associated with poly(styryllithum) was extinguished, indicating crossover to the oxanion. This solution was left to react at 22 °C for 20 h and then terminated with excess trimethylchlorosilane.

The product was recovered from solution by precipitation in a 1:1 volume mixture of methanol and 2-propanol at room temperature. Residual D_3 monomer was washed from the polymer with methanol, followed by drying to a constant weight under vacuum.

Solution ^{1}H NMR was used to independently establish the triblock copolymer composition. A 10 mg/mL deuterated chloroform solution was examined using a Varian 500-MHz instrument. The resulting spectrum is labeled and shown in Figure 2. Based on the integrated intensities, we have determined relative I, S, and D repeat unit mole fractions of 0.45/0.34/0.21, respectively. The molar ratio between I and S agrees well with the reaction stoichiometry. The molar ratio between D and the other two blocks indicates the reaction of D_3 reached approximately 50% conversion, as has been observed for polymerization of PDMS homopolymer under similar conditions.[15] In the remainder of this paper, we will refer to the composition of the ISD triblock on a volume fraction basis. Based on the published homopolymer densities at 413 K[16] and repeat unit molecular weight, the mole fraction composition determined by NMR converts to a volume fraction composition of 0.40/0.41/0.19 for I/S/D.

Gel permeation chromatography (GPC) was used to establish the overall polydispersity of the ISD polymer and to determine I homopolymer or IS diblock copolymer impurities. A Waters 150-C instrument fitted with Phenomenex Phenogel columns operated with $CHCl_3$ as the mobile phase at 22 °C and calibrated with poly(styrene) standards (Polymer Laboratories) was employed. Figure 3 shows the resulting GPC trace. A primary peak is observed, indicating predominately triblock. The small shoulder on the primary peak at short retention times has approximately twice the ISD molecular weight. We attribute this response to the spurious coupling of about 5% of the ISD chains, either prior to termination or during recovery. The overall sample polydispersity (M_w/M_n) is approximately 1.18 relative to poly(styrene) standards.

(10) Park, M.; Harrison, C.; Chaikin, P. M.; Register, R. A.; Adamson, D. H. *Science* **1997**, *276*, 1401.

(11) Hajduk, D. A. Harper, P. E.; Gruner, S. M.; Honeker, C. C.; Kim, G.; Thomas, E. L.; Fetters, L. J. *Macromolecules* **1994**, *27*, 4063−4075.

(12) Ndoni, S.; Papadakis, C. M.; Bates, F. S.; Amdal K. *Rev. Sci Instrum.* **1995**, *66*, 1090−1095.

(13) Rosedale, J. H. Ph.D. Thesis, University of Minnesota, 1993.

(14) Schulz, M. F.; Khandpur, A. K.; Bates, F. S.; Almdal, K.; Mortensen, K.; Hajduk, D. A.; Gruner, S. M. *Macromolecules* **1996**, *29*, 2857−2867.

(15) Maschke, U.; Wagner T.; Coqueret, X. *Mackromol. Chem.* **1992**, *193*, 2453−2466.

(16) Fetters, L. J.; Lohse, D. J.; Richter, D.; Witten, T. A.; Zirkel, A. *Macromolecules* **1994**, *27*, 4639−4646.

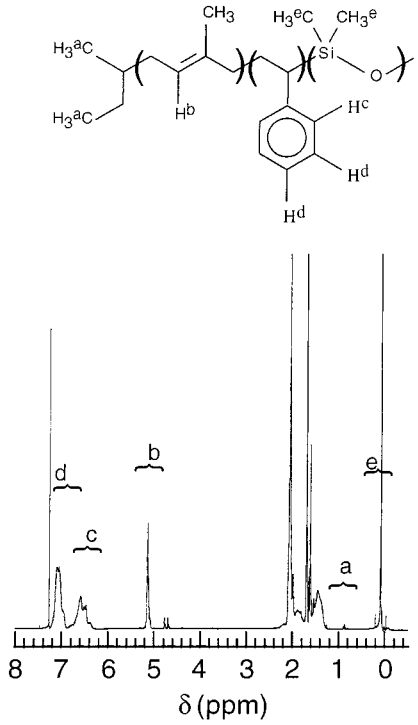

Figure 2. ^{1}H NMR spectra of ISD in $CDCl_3$. The peaks corresponding to specific protons are marked accordingly. The isoprene block is approximately 95% 4,1 addition. The terminal protons from the 4,3 addition of I appear as a doublet at 4.8 ppm.

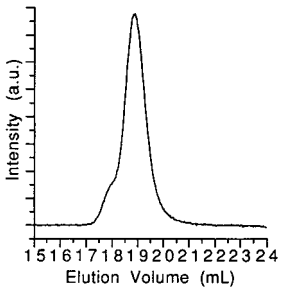

Figure 3. Gel permeation chromatograph of the ISD triblock copolymer taken in chloroform. A polydispersity of 1.18 was calculated on the basis of a poly(styrene) calibration curve. The shoulder at short retention time is most likely associated with a small amount (ca. 5%) of coupled triblock.

We have estimated the overall number-average molecular weight based on the reaction stoichiometry and verified this number with end group analysis in NMR. The molecular weights of the I and S blocks were calculated from the ratios of grams of monomer to moles of initiator. The molecular weight of the D block was calculated by multiplying molar ratio of D to S in NMR by the total number of moles of S reacted and by the repeat unit molecular weight of D and dividing by the number of moles of initiator. This analysis yields $M_n = 41\,000$ g/mol. For end group analysis, the peak corresponding to the protons on the two methyl groups of the *sec*-butyl initiator fragment is integrated, and the molar ratio of end groups to monomers is found for the three blocks. The molecular weight estimated from this method is approximately 5% higher than that expected from reaction stoichiometry. This is within the experimental error of this technique. These estimated values for the molecular weight correspond to an ideal ISD triblock polymerization. Spurious coupling, leading to some IS(DD)SI pentablock, could increase the actual value of M_n. However, comparison of the phase behavior of AB diblocks with A(BB)A triblocks suggests that such coupling has little effect on the sample morphology.[17] Therefore, we ignore this minor complication for the remainder of the report.

Samples were prepared for physical characterization by pressing the powder recovered from the reaction into sheets 1 mm thick at 150 °C under vacuum.

Small-Angle X-ray Scattering. SAXS measurements were performed at the characterization facility of the Center for Interfacial Engineering at the University of Minnesota. Copper Kα radiation of wavelength $\lambda = 1.54$ Å was generated by a Rigaku Ru-200BVH rotating anode using a 0.2×2 mm^2 microfocus cathode and monochromatized by total reflecting Franks mirrors and a nickel foil filter. Two-dimensional diffraction data were collected with a Siemens HI-STAR multiwire area detector located 2.25 m from the sample. All data were corrected for detector response characteristics prior to analysis. The two-dimensional SAXS data were collected at ambient temperature. The powder data were collected at 60 °C.

Small-Angle Neutron Scattering. SANS experiments were conducted at the National Institute of Standards and Technology, Gaithersburg, MD. The neutron wavelength was $\lambda = 6.0$ Å with a spread of $\Delta\lambda/\lambda = 0.10$. Two-dimensional scattering patterns were recorded at a sample-to-detector distance of 7 m, and all data were corrected for background intensity and detector sensitivity prior to analysis. The data were collected at 60 °C.

Transmission Electron Microscopy. TEM images were recorded using a JEOL 1210 TEM operating at 120 kV. The samples were prepared using a Reichart ultramicrotome equipped with a diamond knife. Slices 800 Å thick were cut at −120 °C to minimize deformation of the rubbery PDMS and PI domains. Some samples were stained with the vapor from a 4% aqueous solution of OsO_4 for 10 min to increase the contrast between the poly(isoprene) and two other domains. The remaining experiments relied on the natural contrast of the poly(dimethylsiloxane) versus poly(styrene) and poly(isoprene).

Large-Amplitude Oscillatory Shear (LAOS). Long-range order was induced in the material using a home-built shear device described elsewhere.[18] Samples were sheared for 1 h at 200 °C with an oscillatory strain amplitude of 125% at a frequency of 1.0 rad/s. This process was conducted under a nitrogen atmosphere to minimize sample degradation. Comparison of the GPC traces taken before and after shear showed no detectable differences, indicating that degradation was avoided.

Theory

Self-consistent field theory (SCFT) models the copolymers as incompressible, flexible Gaussian chains with short-range interactions.[2,8,19] The molecular parameters required for the model include the degree of polymerization of each block, N_i (i = I, S, or D), the statistical length, a_i, of each segment, and the standard Flory−Huggins χ_{ij} parameters, specifying the interaction strengths between unlike segments. For convenience, segments are defined on the basis of a common volume, v_o, which we take to be 118 Å^3.[16] In terms of this common segment volume, the degree of polymerization is given by $N_i = M_i/(\rho_i v_o N_A)$, where M_i is the molecular weight of the ith block, ρ_i is the mass density of the ith species, and N_A is Avogadro's number. The statistical segment lengths were calculated using $a_i = (\rho_i v_o N_A \langle r_o^2\rangle_i/M_i)^{1/2}$ and tabulated values of $\langle r_o^2\rangle_i/M_i$, the ratio of the average end-to-end length squared over the molecular weight, measured from homopolymers of type i.[16] The calculated values of N_i and a_i are listed in Table 1. Values for the segment−segment interaction parameters at 150 °C are $\chi_{ID} = 0.09$,[20] $\chi_{SD} = 0.12$,[21] and $\chi_{IS} = 0.033$.[22]

(17) Ryu, C. Y.; Lee, M. S. Hajduk, D. A.; Lodge, T. P. *J. Polym. Sci. Part B: Polym. Phys.* **1997**, *35*, 2811−2823. Matsen, M. W.; Schick, M. *Macromolecules* **1994**, *27*, 6761−6767.

(18) Amdal, K.; Bates, F. S.; Mortensen, K. *J. Chem. Phys.* **1992**, *96*, 9122−9132.

(19) Matsen, M. W.; Bates, F. S. *Macromolecules* **1996**, *29*, 1091−1098.

(20) χ_{ID} was measured by Kristoffer Almdal from the ODT's of two AB diblock copolymers of different molecular weights. Assuming a linear dependence on temperature, $\chi_{ID} = 43.6/T - 0.010$.

(21) χ_{SD} was measured in the same way as χ_{ID}, yielding a temperature dependence $\chi_{SD} = 68.0/T + 0.037$.

Table 1. Physical Parameters for the ISD Triblock Copolymer

block	M_n[a] (g/mol)	ρ_i[b] (g/cm^3)	f_i[c]	N_i	$\langle r_o^2\rangle_i/M_i$[d] (Å^2 mol/g)	a_i[e] (Å)	$\rho_{e,i}$[f] (mol e$^-$/cm^3)	$(b/v)_i$[g] (cm^{-1})
I	14 900	0.830	0.40	252	0.625	6.08	30.2	0.264
S	18 400	0.969	0.41	268	0.434	5.46	33.9	1.41
D	7 700	0.895	0.19	121	0.457	5.38	31.5	0.064

[a] See the Experimental Section for details on how the molecular weight of each block was calculated. [b] Density from ref 16 at 413 K. [c] Volume fraction of block *i*. [d] Ratio from ref 16 for homopolymer *i*. [e] Statistical segment length $a = (\langle r_o^2\rangle/N_i)^{1/2}$. [f] Electron density for SAXS analysis. [g] Scattering length density for SANS analysis.

A complete description of the theory as applied to ABC triblocks can be found in a previous report.[8] In principle, the calculation is fairly straightforward. SCFT represents the molecular interactions experienced by a segment of type *i* at position **r** by a field $w_i(\mathbf{r})$. Then the distribution $\phi_i(\mathbf{r})$ for each segment type is calculated by performing the statistical mechanics of a copolymer molecule subjected to the fields. Since the segment distributions are responsible for creating the fields, there exist self-consistent conditions relating the $\phi_i(\mathbf{r})$ and $w_i(\mathbf{r})$ values. The fields must be adjusted so that these conditions are satisfied. In general, there are many solutions, each representing a different morphology. If we were interested in which is the stable one and which are just metastable, we could calculate their free energies. However, we will only be interested in finding the solution with segment profiles, $\phi_i(\mathbf{r})$, matching our experimental results.

Solving the self-consistent field equations in real space is unfeasible except for the simplest of morphologies. Success requires that all spatially dependent quantities be expanded in Fourier series and that all the equations be expressed in terms of their Fourier coefficients. In practice, calculations are limited to about 400 or 500 Fourier terms. This number of terms is only sufficient at weak degrees of segregation, where the domain interfaces are relatively broad. Well-segregated melts can be addressed only by using generalized Fourier functions which assume a certain space group symmetry of the morphology.[19] For the calculation performed here, this reduces the number of terms required by a factor of $\sim 10^2$, which decreases the computational time by a factor of $\sim 10^8$.

Even with the above advantages, the degree of segregation between the S and D domains is somewhat too large for practical calculations. The value of χ_{ID} would also be a bit too large if it were not for the fact that the structure we find does not have any internal I/D interfaces. Fortunately, we are only interested in the segment profiles or, equivalently, the domain shapes, and these are relatively insensitive to the χ parameters once the domains are nearly pure and the interfaces become well defined.[2] Thus, for our purposes, it is acceptable to use $\chi_{ID} = 0.08$, $\chi_{SD} = 0.08$, and $\chi_{IS} = 0.033$. Note that, if we were interested in determining, for example, the relative stability of various morphologies or the size of their unit cells, then reducing the χ values would not be acceptable. Thus, agreement between theory and experiment in this case indicates that the theoretical solution is a thermodynamically plausible description of the experimental structure. It does not *prove* that a given structure is a uniquely accurate representation of the sample morphology.

Results and Analysis

Two-Dimensional SAXS. After randomly oriented powder specimens, prepared as described above, were subjected to large-amplitude oscillatory shear at temperatures above the glass transition temperature of the poly(styrene) block, alignment of the sample microstructure resulted in the resolution a number of discrete reflections (Figure 4). Both six-fold (Figure 4a) and two-fold (Figure 4c) symmetries were observed, characteristic of either a hexagonal, trigonal, or cubic structure.

When viewed between crossed polarizers at a variety of sample orientations, both sheared and unsheared samples were nonbirefringent. For comparison, ISD copolymers of slightly different compositions but comparable molecular weights that had either lamellar or core−shell cylinder morphologies were strongly birefringent when examined. Thus, the absence of depolarization in the initial material is not due to a low intrinsic birefringence but instead reflects the absence of an optical axis. This, in turn, indicates cubic symmetry.

The scattering data show reflections at relative radial positions of $\sqrt{3}$, $\sqrt{4}$, $\sqrt{7}$, $\sqrt{12}$, and $\sqrt{13}$ (Figure 4a) and $\sqrt{3}$, $\sqrt{4}$, $\sqrt{8}$, $\sqrt{10}$, and $\sqrt{12}$ (Figure 4c). Reflection $\langle hkl\rangle$ for a cubic phase appears at a radial position of mq^*, where $m^2 = h^2 + k^2 + l^2$ is the peak modulus and $2\pi/q^*$ is the edge length of the cubic unit cell. Since 7 is not the sum of three squares, the presence of a reflection at this relative position suggests that the true relative positions are $\sqrt{6}$, $\sqrt{8}$, $\sqrt{14}$, $\sqrt{16}$, $\sqrt{20}$, $\sqrt{24}$, and $\sqrt{26}$. The corresponding Miller indices are $\langle 211\rangle$, $\langle 220\rangle$, $\langle 321\rangle$, $\langle 400\rangle$, $\langle 332\rangle$ or $\langle 420\rangle$, $\langle 422\rangle$, and $\langle 431\rangle$.

The six-fold symmetry seen in Figure 4a identifies this orientation as the [111] projection of the cubic unit cell. In this projection, of the peaks identified earlier, only the $\langle 211\rangle$, $\langle 220\rangle$, $\langle 321\rangle$, $\langle 422\rangle$, and $\langle 431\rangle$ reflections should be observed. The radial positions of these reflections are indicated by white rings in Figure 4a, and almost all of the data fall on the predicted circles to within experimental error. The relative angular positions of these reflections also agree with the predicted values given the indexation shown in Figure 4b. (The angle θ between two reflections is given by $\mathbf{a}\cdot\mathbf{b} = |a||b| \cos\theta$, where **a** and **b** are the vectors defined by the indices of the two reflections.) The pair of $\langle 220\rangle$ reflections that lie along the line parallel to the q_1 axis is more intense than the two other pairs of $\langle 220\rangle$ reflections. This could be caused by a slight rotation of the sample out of the [111] projection. Such a rotation could also bring four $\langle 420\rangle$ spots which lie 15° out of the [111] projection into view, as marked by open circles in Figure 4a,b.

A 90° rotation about the q_2 axis aligns the incident beam along the $[20\bar{2}]$ direction (Figure 4c). (See Figure 4g for the relation between the three scattering planes.) As before, most of the observed reflections appear at the locations expected for the $[20\bar{2}]$ projection of a cubic unit cell. However, there are several visible reflections that appear at the proper radial positions but incorrect angular positions for this orientation. The $\langle 332\rangle$ reflections are indicated by open circles; they belong to other single-crystal domains that are related to the original orientation by twinning. Finally, a 90° rotation about the q_1 axis aligns the beam along the $[\bar{1}2\bar{1}]$ direction (Figure 4e). However, the observed diffraction is most consistent with the $[\bar{1}3\bar{1}]$ direction; the 10° angle between these projections is within the experimental uncertainty afforded by our simple sample mounting procedure.

(22) Hashimoto, T.; Ijichi, Y.; Fetters, L. J. *J. Chem. Phys.* **1988**, *89*, 2463−2472.

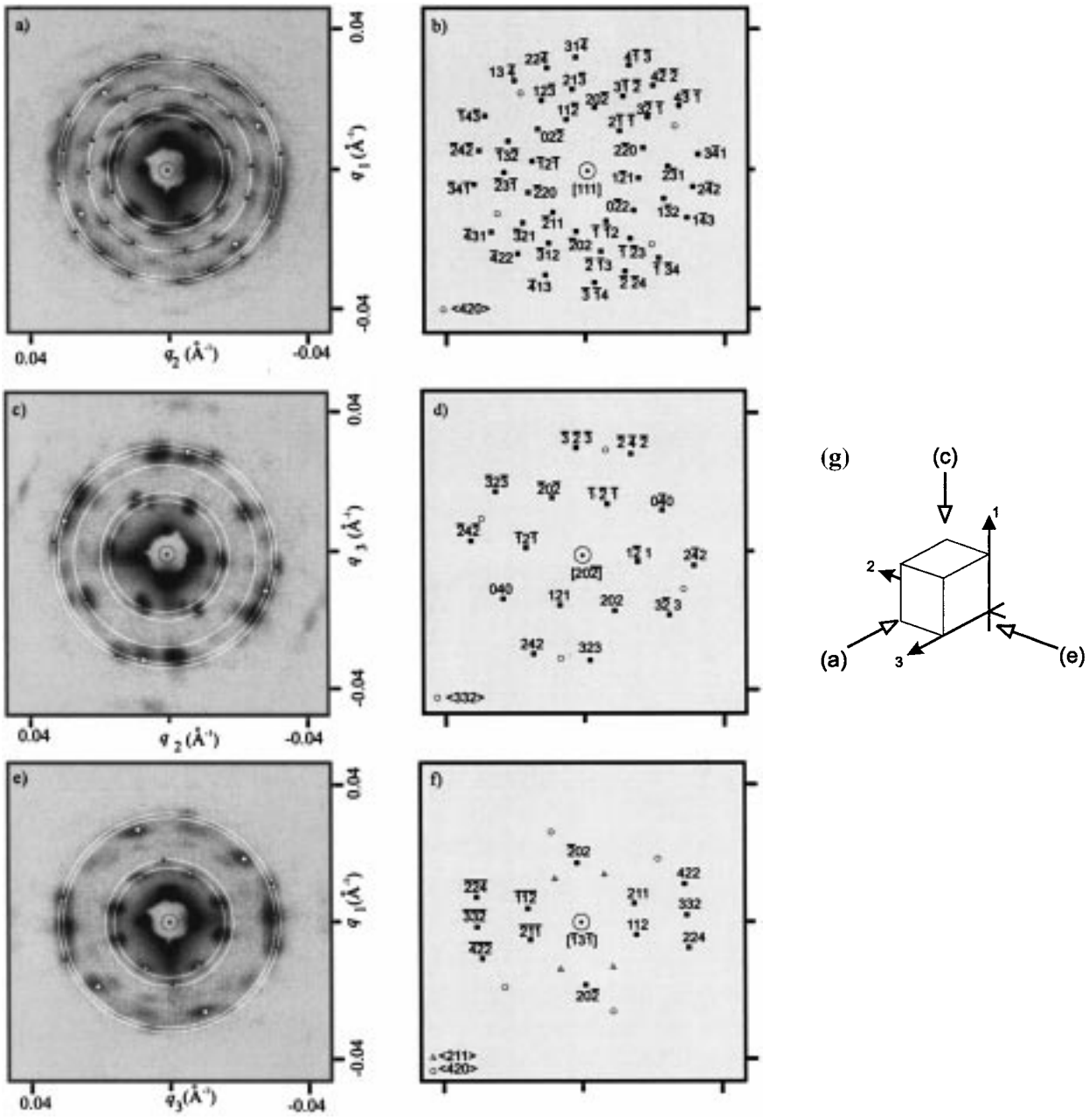

Figure 4. SAXS diffraction patterns obtained from a sheared sample of ISD. (a) This pattern is consistent with diffraction from {111} planes with $Ia\bar{3}d$ space group symmetry. The rings indicate the predicted positions of the higher order reflections relative to the lowest order ⟨211⟩ reflections. With increasing diameter, the rings correspond to the ⟨211⟩, ⟨220⟩, ⟨321⟩, ⟨422⟩, and ⟨431⟩ reflections. (b) Single-crystal indexation for (a) is shown by dark squares. The white circles correspond to the ⟨420⟩ reflections that lie 15° out of the [111] projection. (c) This diffraction pattern was obtained after the sample was rotated 90° about the q_2 axis from its position in (a). This set of reflections is consistent with diffraction from {20$\bar{2}$} planes of a sample having $Ia\bar{3}d$ symmetry, where the rings correspond to the ⟨211⟩, ⟨220⟩, ⟨400⟩, ⟨332⟩, and ⟨224⟩ reflections. (d) The single-crystal indexation of the [20$\bar{2}$] direction (filled squares) based on $Ia\bar{3}d$ symmetry. Open circles correspond to spots that lie on the ⟨332⟩ ring but cannot be indexed by a single-crystal pattern. Their positions are consistent with a twinned structure. (e) Diffraction pattern obtained after rotating the sample in (a) approximately 90° around the q_3 axis. This pattern is most consistent with reflections from the {131} planes of a sample having $Ia\bar{3}d$ symmetry. A 10° misalignment during sample mounting can account for the observed [$\bar{1}3\bar{1}$] rather than the expected [$\bar{1}2\bar{1}$] direction. The rings correspond to ⟨211⟩, <202>, ⟨332⟩, and ⟨224⟩ reflections. (f) The dark squares correspond to the single-crystal indexation of the [$\bar{1}3\bar{1}$] direction. The open triangles are out-of-plane ⟨211⟩ reflections, and the open circles are out-of-plane ⟨420⟩ reflections. (g) Schematic showing the relationship between axes of rotation and scattering planes for (a), (c), and (e).

The reflections observed are consistent with all the extinction symbols having the *P* or *I* symmetry. Space groups with the *F* symmetry are not allowed by the appearance of the ⟨211⟩ reflctions in Figure 4. Since many of the *P* and *I* space groups share a number of permitted reflections, differentiation of these symmetries on the basis of diffraction data is challenging. The absence of a particular reflection is not cause for the rejection of a particular group, as it may be caused by a minimum in the Fourier transform of the unit cell electron density. However, it is unlikely that a large number of reflections can be extinguished in this manner. Thus, it is the general pattern of agreement between the predicted and observed data that determines whether we reject or accept a given assignment.

A large number of lower-order reflections that are allowed in the space groups with the *P* symmetry and *I*..., $I4_1$.., and *Ia*.. extinction symbols are not observed in this sample. The data

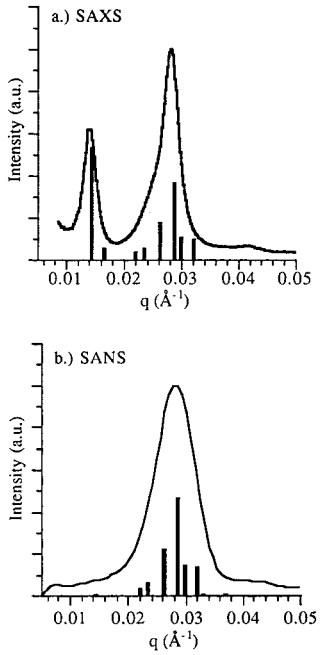

Figure 5. (a) Small-angle X-ray scattering (solid curve) powder diffraction patterns obtained from the ISD triblock copolymer. Black histogram bars represent the calculated intensities of the reflections based on the SCFT core−shell gyroid ($Ia\bar{3}d$) morphology. (b) Small-angle neutron scattering (solid curve) powder diffraction patterns obtained from the ISD triblock copolymer. Black histogram bars represent the reflections' intensities from theory. Agreement between the experiment and theory regarding the presence and extinction of the first-order reflection in SAXS and SANS, respectively, provides confirmation of the assigned morphology.

are most consistent with $Ia\bar{3}d$ and $I\bar{4}3d$ symmetries. Within the first eight reflections, the only differences in the allowed reflections of these two groups are the ⟨310⟩ reflections which appear in the $I\bar{4}3d$ symmetry but are not allowed in the $Ia\bar{3}d$ space group. Unfortunately, if the ⟨310⟩ reflections were present, they would not appear in the [111], [20$\bar{2}$], or [$\bar{1}3\bar{1}$] projections presented here. Thus, based on these data, we are only able to reduce the number of probable space groups to two: $I\bar{4}3d$ or $Ia\bar{3}d$.

Powder Diffraction. SAXS was performed on macroscopically isotropic samples prepared by pressing the powder as described above. The two broad maxima in the diffraction pattern (shown as a solid line in Figure 5a) suggest the superposition of multiple reflections. Fortunately, our 2-D SAXS analysis has narrowed the number of possible space groups to two. Since the first two allowed reflections in the $I\bar{4}3d$ and $Ia\bar{3}d$ space groups are the same, we can fit the first peak in the powder data to the sum of two Gaussian distributions representing the ⟨211⟩ and ⟨220⟩ reflections. The center of the first Gaussian is 0.0143 Å^{-1}, corresponding to a d spacing of the {211} planes equal to 440 Å and a unit cell size of 1080 Å.[23] The ⟨310⟩ reflections in a sample having $I\bar{4}3d$ symmetry would appear at a position of 0.0185 Å^{-1}. There is a minimum in the powder pattern at this position, indicating that the pattern is consistent with the $Ia\bar{3}d$ symmetry. However, the intensity of reflections from the $I\bar{4}3d$ symmetry could be minimized by the structure factor. Because only the appearance of reflections proves a sample belongs to a particular space group, we are unable to conclude from the SAXS data alone to which space group this sample belongs.

SANS provided a complementary powder diffraction pattern from the same isotropic specimen, and the one-dimensional result is presented in Figure 5b as a solid line. Immediately apparent are the gross differences between the SAXS and SANS results. Specifically, the leading order reflections in the SAXS pattern are completely absent in the SANS data. We consider these differences in the following sections.

TEM. The results of the scattering experiments yielded two likely symmetries of the sample but not a unique morphology. We therefore employed TEM to determine how the three blocks fill space. As can be seen in Figure 6a, the silicon in the D blocks provides natural contrast, in which the dark regions correspond to D and appear to be arranged in a continuous network. The nearly three-fold symmetric "wagon wheel" pattern is reminiscent of the {111} planes of the gyroid morphology in diblock copolymers.[11] In the {111} planes of the gyroid morphology, the "spokes" of the "wagon wheels" are the same length.[11] We attribute the distortion in our image to a slight amount of misorientation. The length of a "spoke" in the three-dimensional structure was calculated from the simple trigonometric relationships between the average lengths of three of the foreshortened "spokes" in the TEM image, giving an actual "spoke" length of 830 Å.

When the I blocks are stained with OsO_4, the sample acquires a second, distinctly different contrast distribution. In Figure 6b, roughly the same axis is shown as in Figure 6a, but the image is now white circles encased in black and arranged in a honeycomb pattern on a gray background. Work with two-dimensionally ordered core−shell ISD cylinders has taught us that the white, gray, and black regions correspond to S, D, and I domains, respectively.[24] However, in this complicated morphology, the gray regions are nearly indistinguishable from the black ones due to a convolution of mass thickness contrast. Thick regions of gray D can have similar contrast to thin regions of black I. As in the unstained samples, the image is observed slightly off a ⟨111⟩ axis. The center-to-center distance in the honeycomb pattern was calculated to be 860 Å using the same trigonometric relationship as in the "wagon wheel" pattern. This value agrees well with the "spoke" length in the unstained image. While this image does not allow us to distinguish the positions of the three domains, it is useful in confirming the calculated structure, as shown below.

We find good agreement between the dimensions of the unit cell as measured by SAXS and TEM. Twice the spacing of the {211} planes corresponds to the "spoke" length observed in TEM. The 880 Å length of the "spoke" predicted by SAXS is close to the 830 and 860 Å observed in stained and unstained TEM images, respectively.

The diffraction patterns from SAXS and SANS are consistent with two space groups, $I\bar{4}3d$ and $Ia\bar{3}d$. To our knowledge, a morphology having the $I\bar{4}3d$ symmetry has not been observed in block copolymers or other self-assembled soft materials, while the well-established gyroid morphology observed in block copolymers belongs to the $Ia\bar{3}d$ space group. The unstained TEM image is consistent with the gyroid morphology, comprised of two interpenetrating and three-fold-connected D networks. To determine this complicated morphology, we turn to SCFT and focus on the $Ia\bar{3}d$ space group based on these experimental observations.

(23) In an experiment reproducing the shear alignment of a different sample, we observed that the ⟨211⟩ peak position shifts to slightly (ca. 4%) higher q values after shear has been applied. Thus, the spacing between the ⟨211⟩ planes (d_{211}) in the sheared sample is ca. 4% smaller than the spacing in the powder sample. In this experiment, both the sheared data and powder data were analyzed at ambient temperature. We are currently studying the cause of the slight decrease in domain spacing due to shear.

(24) Shefelbine, T. A.; Bates, F. S.; Fredrickson, G. H. Unpublished data.

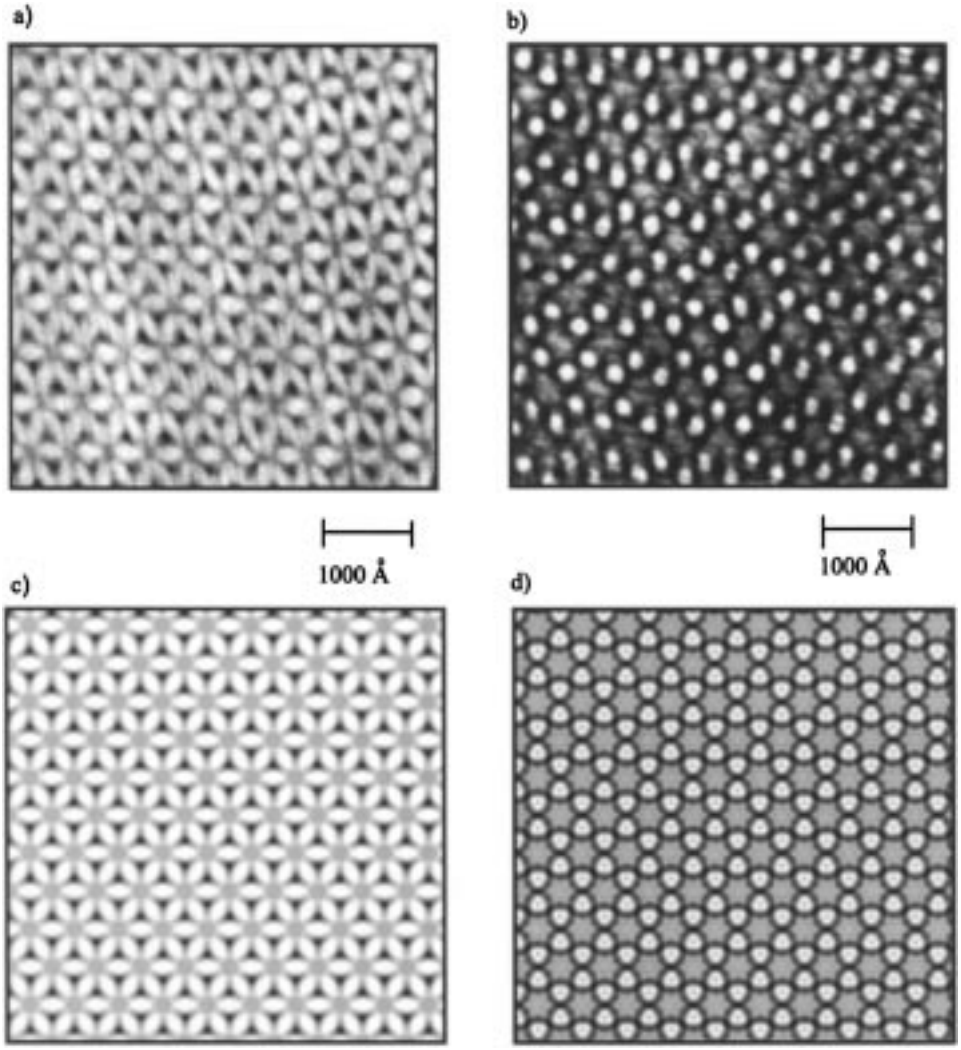

Figure 6. (a) TEM image taken from an unstained thin section of the ISD triblock copolymer. Natural contrast renders the poly(dimethylsiloxane) (D) domains dark, while the poly(isoprene) (I) and poly(styrene) (S) domains appear white. The "wagon wheel" pattern is associated the two D networks arranged in a gyroid morphology. (b) TEM micrograph obtained from an OsO_4 stained thin section of ISD. Staining selectively darkens the I domains relative to the gray D and white S domains. Both micrographs represent nearly the same projections along the [111] direction of the cubic morphology. (c and d) Projections of a thin section of the core−shell gyroid SCFT model calculation along the [111] direction. The relative mass density contrast has been weighted in (c) and (d) to correspond to the experimental conditions in (a) and (b), respectively.

Theory. The objective now is to find the morphology that matches the scattering and TEM data. By using the SCFT described above, we can accurately predict the domain shapes of our triblock copolymer morphology associated with specific ordered state symmetries. The only parameters needed for the calculation, N_i, a_i, and χ_{ij}, are listed in the Theory section and Table 1. To perform the calculation, knowledge of the space-group symmetry is required, and so we consider the most likely candidate, $Ia\bar{3}d$. As discussed in the Theory section, the SCFT requires us to solve self-consistent field equations by an iterative technique, which requires an initial guess for the fields. To obtain an appropriate guess, we used the TEM evidence (Figure 6a) that the D domains formed two interweaving lattices analogous to those in the gyroid phase of simple diblock copolymers. It was also helpful to start our calculation at a fairly low degree of segregation, where the convergence is better and where fewer Fourier functions are required. Once a solution was found, the degree of segregation was increased as far as possible, as discussed above. The resulting morphology is shown in Figure 7. Now we must confirm that the theoretical morphology agrees with the experimental data.

The powder diffraction intensities are immediately obtained from the Fourier coefficients of the segment densities, $\phi_i(\mathbf{r})$. Each Fourier term corresponds to a particular $\langle hkl \rangle$ reflection.[19] To calculate a relative X-ray scattering intensity for a given reflection, the corresponding Fourier coefficients for the three components are weighted by their respective electron densities ($\rho_{e,i}$ in Table 1), summed, and then squared. We do not have to correct for the multiplicity in these calculations because we are using generalized Fourier functions. The Lorentz correction is applied because we are sampling a two-dimensional ring of a three-dimensional shell in reciprocal space; therefore, the intensity of each reflection is divided by its modulus.[25] The resulting intensities are then scaled by a constant to match the scale of the experimental pattern. The q value for each theoretical reflection is taken as $m/\sqrt{6}$ times 0.0143 $Å^{-1}$, which is the position of the lowest-order {211} reflection. The predictions are shown as dark histogram bars in Figure 5a. Although the resolution of the experiment was insufficient to identify the individual peaks, there is a reasonable correspondence between the predicted intensities and the experi-

(25) Warren, B. E. *X-ray Diffraction*; Addison-Wesley Publishing Co.: Menlo Park, CA, 1968; p 49.

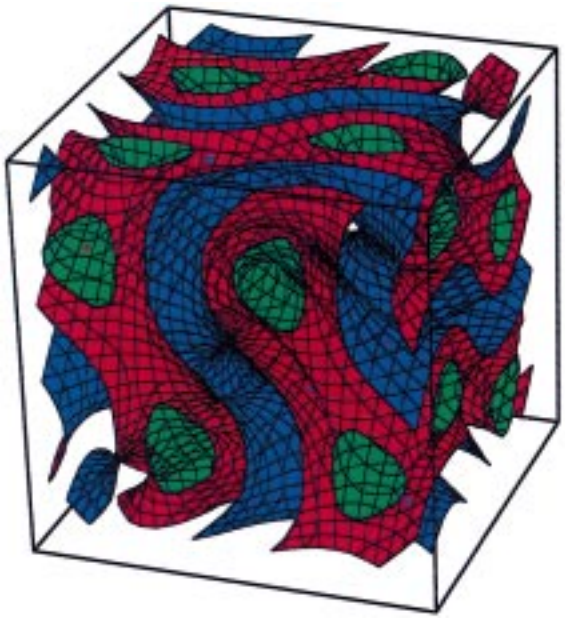

Figure 7. Self-consistent field theory solution to the ISD triblock copolymer core−shell gyroid morphology; I, S, and D regions (colored blue, red, and green) make up 40, 41, and 19 vol % of the material, respectively. This illustration shows the intermaterial dividing surfaces within one $Ia\bar{3}d$ unit cell. Two three-fold-connected D networks are each surrounded by S domains that are separated by an I domain, resulting in a triply periodic pentacontinuous morphology. See Figure 1 for an alternative depiction of the overall topology of this structure.

mental SAXS pattern. Considering the inaccuracy in the model parameters (particularly the χ values) and the uncertainty associated with the electon densities of the three components, there is reasonable agreement between the predicted and measured intensities. The predicted intensities for neutron scattering are obtained in the same manner, except that the Fourier coefficients are weighted by neutron cross sections ($(b/v)_i$ in Table 1). The SANS predictions are shown in Figure 5b with dark histogram bars. Remarkably, there is almost perfect accidental cancellation of the first two peaks, as found experimentally. The simultaneous agreement for both scattering experiments is convincing evidence that the theory has located the correct morphology.

From the theoretical domain profiles, it is a simple task to generate simulated TEM images. To obtain three-fold symmetry, we examined slices of the model orthogonal to the [111] direction. The slice thickness was chosen to be one repeat period, which corresponds to ~930 Å for $Ia\bar{3}d$ with a unit cell size of 1080 Å, because slices of this thickness produce the same image regardless of their position relative to the unit cell.[8] This theoretical thickness is close to the thicknesses of the TEM samples, 800 Å. To compare the theory with the unstained image, we set the S and I microdomains to be transparent, while D is dark. These contrast levels are analogous to the TEM images, where I and S scatter fewer electrons and appear white, while D scatters more electrons and appears dark. The simulated TEM image in Figure 6c captures the important features of the experimental image in Figure 6a. The pattern of "wagon wheels" has six white "spokes" originating from each dark "hub". The theoretical stained image is obtained by setting the contrast of I to be twice that of D, while S remains transparent. These levels of contrast have been observed in other simple morphologies with I, S, and D blocks.[24] The result is the image in Figure 6d, which agrees well with the experimental one in Figure 6b. The strong resemblance of theory to experiment for two types of contrast mechanisms is further evidence that the structure depicted in Figure 7 correctly describes the morphology of ISD.

Discussion

The structure reported here divides space into five distinct regions that are each continuous in three dimensions. The two D cores (the green domains in Figures 1 and 7) form the two independent, interweaving networks of three-fold connectors. The S shells (in red) surrounding each core add two more distinct subdivisions, and I (in blue) fills the remaining space. Thus, the morphology can be described as pentacontinuous, meaning the five distinct domains are each continuous in all three dimensions. To distinguish this morphology from the other gyroid morphologies that have been observed, we will refer to it as G^3_5. The superscript indicates the number of chemically distinct blocks and the subscript indicates the number of independent, continuous domains. The gyroid structure observed in AB diblock and ABA triblock copolymers has three distinct domains from two types of blocks and is commonly called tricontinuous. In our notation, this structure is referred to as G^2_3. Previous ABC triblock copolymers observed with a gyroid-like structure have three distinct domains and belong to the $I4_132$ space group.[5,8] In this structure, each end block forms one of the independent networks of three-fold connectors breaking the $Ia\bar{3}d$ symmetry. Thus, the structure is tricontinuous with three chemical species, or G^3_3.

The core−shell gyroid phase identified here is a sensible equilibrium structure for our particular triblock copolymer. The S domain completely separates the I and D domains, as it should given the block sequence and volume fractions of the copolymer. Previous ABC triblocks[7] have produced A−C interfaces but only when the middle block was small and highly incompatible with the end blocks; that situation does not occur here. Furthermore, it is reasonable to expect a core−shell structure with D at the center since this type of structure allows the costly S−D interface to be much smaller than the S−I interface. Also, the inner S−D interface has a significant interfacial curvature, while the outer surface is much flatter. This nicely satisfies the preferred interfacial curvatures expected for $f_D < f_S$ and $f_S \cong f_I$, respectively. The overall interfacial curvature would tend to increase as the ratios χ_{S-D}/χ_{S-I}, f_S/f_D, and f_I/f_S are increased. This should cause a progression from lamellae, to core−shell gyroid, to core−shell cylinders, to core−shell spheres analogous to the sequence observed in diblock copolymers.[26] Apparently, the ratios in this polymer are such that core−shell gyroid provides the best overall curvature.

This polymer represents one point in a multidimensional phase space defined by composition, N_i, and segregation parameters χ_{ij} for i,j = I, S, or D. Studies are currently underway to examine how the three χ_{ij} parameters influence the morphologies of ISD triblocks with different compositions. Preliminary studies on this system suggest that the composition window for the core−shell gyroid morphology is narrow. A narrow composition window is expected because the core−shell cylinder phase is hexagonally packed and has a small degree of packing frustration.[8] This contrasts with previous studies of symmetric ABC triblocks in which the multicontinuous structure G^3_3 exists over a wider composition range than G^2_3 phase in diblocks. In the system that exhibits the G^3_3 phase, the tetragonally packed cylinder phase has a large amount of packing frustration, which reduces the composition window of tetragonal cylinders and increases that of G^3_3.

(26) Bates, F. S.; Fredrickson, G. H. *Phys. Today* **1999**, *52* (2), 32−38.

Another unusual feature of this polymer is the ability of shear to induce long-range order in a gyroid structure. In AB copolymers, the inability of shear to align the G morphology has been associated with the spatially isotropic nature of the morphology and the corresponding absence of an "easy-flow" direction. Ordered G phases have been observed when the G phase grows from other shear aligned phases (cylinders or lamellae) upon changing temperature.[27] In this polymer, a similar phase transition may take place. As the polymer is heated, a lower symmetry phase may form that develops long-range order under shear. Core−shell cylinders[28] or spheres[29] are each a possibility, as both domain types (cylinders and spheres) are known to develop long-range order under dynamic shear in diblock copolymers. Epitaxial transformation to the G_5^3 phase upon cooling would preserve long-range order. When the S domain becomes glassy, the structure would become fixed. Studies are currently underway to evaluate this hypothesis.

The high interfacial area that characterizes this structure and the configuration of glassy and rubbery blocks make this material an exciting candidate for membrane applications. Glassy polymers exhibit good permeate selectivity but low permeability, while rubbers have poor selectivity but high permeability. At every point in the bulk structure, the glassy S shells separate the rubbery D and I blocks. The interfacial area per unit volume between the glassy S and rubbery D and I is high, approximately 10^6 cm^2/cm^3, offering a potentially huge area for selective permeation. For a block copolymer membrane with very high selective area per volume to work, the rubbery blocks on the upstream and downstream sides must be separated everywhere by the glassy, selective block. Separation will then be effected by facile penetration through D, selective diffusion through S, followed by collection from the I domain.

In the bulk structure, the core-in-shell gyroid material meets these requirements. If the surface morphology of the membrane can be controlled so that one rubbery block appears on the upstream surface and the other on the downstream surface, a membrane with very high selective area per volume will be achieved. A triblock membrane with an area of 1 cm^2 and thickness of 10 μm has a total selective area of 10^3 cm^2. We do not expect the flow through the triblock membrane to be 10^3 times greater than that through a flat membrane constructed from the same materials because the driving force for permeation decreases through the thickness of the membrane. Calculations analogous to the Thiele calculation of catalytic reaction in a porous pellet[30] indicate that the flux through an ISD membrane with selective S area, like that identified here, should function with approximately a 10-fold enhancement in performance over the corresponding flat membrane made from the same materials. This represents a considerable gain, provided the triblock can be configured into defect-free and mechanically robust films. We are currently exploring these issues.

Conclusion

We have used a comprehensive set of experimental and theoretical techniques to characterize a core−shell gyroid morphology in a poly(isoprene-*block*-styrene-*block*-dimethylsiloxane) ABC triblock copolymer. From two-dimensional SAXS of shear-oriented samples, we determined two possible space groups, $Ia\bar{3}d$ and $I\bar{4}3d$. In TEM images of unstained samples, we observed patterns reminiscent of the gyroid morphology seen in diblocks. From these data, we chose to perform SCFT calculations for a model of the polymer having the $Ia\bar{3}d$ space group symmetry. The results of this model agree very well with the TEM images and powder SANS and SAXS diffraction patterns, indicating the model describes the actual morphology. A three-dimensional rendition of the model demonstrates that the morphology of this sample is core−shell gyroid with poly(dimethylsiloxane) cores, surrounded in poly(styrene) shells, and embedded in a poly(isoprene) matrix.

Acknowledgment. The authors acknowledge Kristoffer Almdal of Risø National Laboratories in Denmark for providing measurements of χ_{ID} and χ_{SD}. Support for this research was provided by the NSF (CTS-9627361 and DMR-94050101). T.A.S. was supported in part by an NSF Graduate Fellowship. M.E.V. gratefully acknowledges the support of the Carlsberg Foundation and The Danish Technical Research Council. M.W.M. was supported by a NUF-NAL grant from the Nuffield Foundation. Calculations were performed at the High Performance Computing Centre at the University of Reading.

JA991442H

(27) Schulz, M. F.; Bates, F. S. Almdal, K.; Mortensen, K. *Phys. Rev. Lett.* **1994**, *73*, 86−89. Förster, S.; Khandpur, A. K.; Zhao, J.; Bates, F. S.; Hamley, I. W.; Ryan, A. J.; Bras, W. *Macromolecules* **1994**, *27*, 6922−6935. Vigild, M. E.; Almdal, K.; Mortensen, K.; Hamley, I. W.; Fairclough, J. P. A.; Ryan, A. J. *Macromolecules* **1998**, *31*, 5702−5716.

(28) Albalak, R. J.; Thomas, E. L. *J. Polym. Sci. Part B: Polym. Phys.* **1993**, *31*, 37−46. Winey, K. I.; Patel, S. S.; Larson, R. G.; Watanabe, H. *Macromolecules* **1993**, *26*, 2542−2549.

(29) Almdal, K.; Koppi, K. A.; Bates, F. S. *Macromolecules* **1993**, *26*, 4058−4060. Koppi, K. A.; Tirrell, M. V.; Bates, F. S.; Almdal, K.; Mortensen, K. *J. Rheol.* **1994**, *38*, 999−1027.

(30) Gronda, A. M.; Buechel, S.; Cussler, E. L. *J. Membr. Sci*., in press.

(31) Seddon, J. M. *Biochim. Biophys. Acta* **1990**, *1031*, 1−69.